Inorganic Chemistry
Article

Inorg. Chem. **2009**, *48*, 9819–9830 **9819**
DOI: 10.1021/ic901330y

Rare Sandwich-Type Polyoxomolybdates Constructed from Di-/Tetra-Nuclear Transition-Metal Clusters and Trivacant Keggin Germanomolybdate Fragments

Suzhi Li, Junwei Zhao, Pengtao Ma, Juan Du, Jingyang Niu,* and Jingping Wang*

Institute of Molecular and Crystal Engineering, College of Chemistry and Chemical Engineering, Henan University, Kaifeng, Henan 475004, P.R. China

Received July 10, 2009

Two types of rare sandwich-type germanomolybdates $[Na_{12}(H_2O)_{36}][Cu_2(\beta\text{-Y-}GeMo_9O_{33})_2]\cdot 3H_2O$ (**1**), $[N(CH_3)_4]_4[Na_6(H_2O)_{24}][Cr_2(\beta\text{-Y-}GeMo_9O_{33})_2]\cdot 7H_2O$ (**2**), and $[Na_{11}(H_2O)_{25}]H[M_4(H_2O)_2(\alpha\text{-B-}GeMo_9O_{34})_2]\cdot 6H_2O$ (M = Ni^{II} for **3**, M = Mn^{II} for **4** and M = Co^{II} for **5**) have been synthesized and characterized by elemental analyses, ICP spectra, IR spectroscopy, UV spectroscopy, thermogravimetry (TG) analyses (for **1**−**3**), X-ray photoelectron spectroscopy (XPS) (for **1** and **3**), X-ray powder diffraction (XRPD) (for **1** and **3**) and single-crystal X-ray diffraction. To our knowledge, **1**−**5** represent the first sandwich-type germanomolybdates containing both $\{\beta\text{-Y-}GeMo_9O_{33}\}$/$\{\alpha\text{-B-}GeMo_9O_{34}\}$ fragments and transition-metal clusters. Interestingly, **1** and **2** display the rare dinuclear transition-metal substituted sandwich-type structures with unusual trivacant $\{\beta\text{-Y-}GeMo_9O_{33}\}$ germanomolybdate units whereas **3**−**5** exhibit the first tetranuclear transition-metal substituted sandwich-type structures with familiar trivacant $\{\alpha\text{-B-}GeMo_9O_{34}\}$ germanomolybdate units. Surface photovoltage spectroscopy (SPS) and electric field induced surface photovoltage spectroscopy (EFISPS) measurements reveal that **1** and **3** bear the behavior of the *n*-type semiconductor. Magnetic measurements indicate **1** and **3** demonstrate antiferromagnetic exchange interactions and ferromagnetic exchange interactions, respectively.

Introduction

Designed synthesis and exploitation of novel transition-metal (TM) substituted polyoxometalates (POMs) has attracted considerable attention in recent years not only for their enormous structural diversities and topological beauty but also for their potential applications in the fields of catalysis, sorption, electrochemistry, optics, medicine, magnetism, and functional materials.[1,2] Recently, more attention has been paid to the preparation and characterization of TM-substituted heteropolytungstates (HPTs) by reaction of TM cations and lacunary POM precursors derived from Keggin and Dawson polyoxoanions (monovacant: $[\alpha\text{-}PW_{11}O_{39}]^{7-}$, $[\alpha\text{-}P_2W_{17}O_{61}]^{10-}$; divacant: $[\gamma\text{-}SiW_{10}O_{36}]^{8-}$; trivacant: $[\alpha\text{-}PW_9O_{34}]^{9-}$, $[\alpha\text{-}P_2W_{15}O_{56}]^{12-}$; etc.) under conventional aqueous solutions or hydrothermal conditions.[3−9] To date, most of the reported compounds are sandwich-type TM-substituted HPTs based on trivacant Keggin units, which usually consist of a TM cluster and two trivacant POM units. The common trivacant POM units include: $[SiW_9O_{34}]^{10-}$,[3] $[PW_9O_{34}]^{9-}$,[3e] $[AsW_9O_{33}]^{9-}$,[4] $[SeW_9O_{33}]^{8-}$,[4b,c] $[GeW_9O_{34}]^{10-}$,[3e,f,5] $[SbW_9O_{33}]^{9-}$,[4b−d,6] $[BiW_9O_{33}]^{9-}$,[6a] $[TeW_9O_{33}]^{8-}$,[4b,c,6a] $[NiW_9O_{34}]^{12-}$.[7a] Main typical

*To whom correspondence should be addressed. E-mail: jyniu@henu.edu.cn, (J.N.), jpwang@henu.edu.cn (J.W.). Fax: (+86) 378 3886876.

(1) (a) *Polyoxometalate Chemistry: From Topology via Self-Assembly to Applications*; Pope, M. T., Müller, A., Eds.; Kluwer: Dordrecht, The Netherlands, 2001; (b) *Polyoxometalate Molecular Science*; Borrás-Almenar, J. J., Coronade, E., Müller, A., Pope, M. T., Eds.; Kluwer: Dordrecht, The Netherlands, 2004.

(2) (a) *Polyoxometalates*; Hill, C. L., Ed.; *Chem. Rev*. **1998**. (b) Pope, M. T. *Comput. Coord. Chem. 2*. **2003**, *4*, 635. (c) Hill, C. L. *Comput. Coord. Chem. 2*. **2003**, *4*, 679.

(3) (a) Kortz, U.; Isber, S.; Dickman, M. H.; Ravot, D. *Inorg. Chem*. **2000**, *39*, 2915. (b) Laronze, N.; Marrot, J.; Hervé, G. *Inorg. Chem*. **2003**, *42*, 5857. (c) Bi, L. H.; Kortz, U. *Inorg. Chem*. **2004**, *43*, 7961. (d) Bi, L. H.; Kortz, U.; Keita, B.; Nadjo, L.; Borrmann, H. *Inorg. Chem*. **2004**, *43*, 8367. (e) Zhao, J. W.; Li, B.; Zheng, S. T.; Yang, G. Y. *Cryst. Growth Des*. **2007**, 2658. (f) Zhao, J. W.; Wang, C. M.; Zhang, J.; Zheng, S. T.; Yang, G. Y. *Chem.—Eur. J*. **2008**, 9223. (g) Weakley, T. J. R.; Evans, H. T., Jr.; Showell, J. S.; Tourné, G. F.; Tourné, C. M. *J. Chem. Soc., Chem. Commun*. **1973**, 139.

(4) (a) Mialane, P.; Marrot, J.; Rivière, E.; Nebout, J.; Hervé, G. *Inorg. Chem*. **2001**, *40*, 44. (b) Kortz, U.; Al-Kassem, N. K.; Savelieff, M. G.; Al Kadi, N. A.; Sadakane, M. *Inorg. Chem*. **2001**, *40*, 4742. (c) Kortz, U.; Savelieff, M. G.; Bassil, B. S.; Keita, B.; Nadjo, L. *Inorg. Chem*. **2002**, *41*, 783. (d) Hussain, F.; Reicke, M.; Kortz, U. *Eur. J. Inorg. Chem*. **2004**, *43*, 2733. (e) Kortz, U.; Nellutla, S.; Stowe, A. C.; Dalal, N. S.; Tol, J. V.; Bassil, B. S. *Inorg. Chem*. **2004**, *43*, 144.

(5) (a) Kortz, U.; Nellutla, S.; Stowe, A. C.; Dalal, N. S.; Rauwald, U.; Danquah, W.; Ravot, D. *Inorg. Chem*. **2004**, *43*, 2308. (b) Bi, L. H.; Kortz, U.; Nellutla, S.; Stowe, A. C.; Tol, J.; Dalal, N. S.; Keita, B.; Nadjo, L. *Inorg. Chem*. **2005**, *44*, 896. (c) Zhao, J. W.; Zhang, J.; Song, Y.; Zheng, S. T.; Yang, G. Y. *Eur. J. Inorg. Chem*. **2008**, 3809. (d) Zhao, J. W.; Zheng, S. T.; Li, Z. H.; Yang, G. Y. *Dalton Trans*. **2009**, 1300. (e) Zhao, J. W.; Han, Q. X.; Ma, P. T.; Chen, L. J.; Wang, J. P.; Niu, J. Y. *Inorg. Chem. Commun*. **2009**, DOI: 10.1016/j.inoche.2009.05.023.

(6) (a) Bösing, M.; Nöh, A.; Loose, I.; Krebs, B. *J. Am. Chem. Soc*. **1998**, *120*, 7252. (b) Volkmer, D.; Bredenkötter, B.; Tellenbröker, J.; Kögerler, P.; Kurth, D. G.; Lehmann, P.; Schnablegger, H.; Schwahn, D.; Piepenbrink, M.; Krebs, B. *J. Am. Chem. Soc*. **2002**, 10489. (c) Bi, L. H.; Reicke, M.; Kortz, U.; Keita, B.; Nadjo, L.; Clark, R. J. *Inorg. Chem*. **2004**, *43*, 3915.

Published on Web 09/21/2009

sandwich-type TM-substituted HPTs are summarized: dinuclear: $[Cs_2K(H_2O)_7Pd_2WO(H_2O)(A\text{-}\alpha\text{-}SiW_9O_{34})_2]^{9-}$,[3d] $[(\alpha\text{-}As W_9O_{33})_2WO(H_2O)M_2(H_2O)_2]^{10-}$ (M = $Zn^{II}/Mn^{II}/Co^{II}$),[4b] and trinuclear: $[(\alpha\text{-}XW_9O_{33})_2M_3(H_2O)_3]^{n-}$ (M = $Cu^{II}/Zn^{II}/Mn^{II}/Co^{II}$; X = $As^{III}/Sb^{III}/Se^{IV}/Te^{IV}$),[4a,4b,6a,6b] and $[Zr_3(OH)_3(A\text{-}\beta\text{-}SiW_9O_{34})_2]^{11-}$;[7m] tetra-nuclear: $[\{SiM_2W_9O_{34}(H_2O)\}_2]^{12-}$ (M = $Mn^{II}/Cu^{II}/Zn^{II}$);[3a] $[Ni_4(Hdap)_2(\alpha\text{-}B\text{-}H_mXW_9O_{34})_2]^{n-}$ (m = 1, X = Si^{IV}/Ge^{IV}; m = 0, X = P^V),[3e] $[Fe_4(H_2O)_{10}(\beta\text{-}XW_9O_{33})_2]^{n-}$ (X = $As^{III}/Sb^{III}/Se^{IV}/Te^{IV}$),[4c] $[Mn(H_2O)_3)_2(Mn(H_2O)_2)_2(TeW_9O_{33})_2]^{8-}$,[6a] $[Ni_4(H_2O)_2(\alpha\text{-}NiW_9O_{34})_2]^{16-}$[7a] and $[M_4(H_2O)_2(XW_9O_{34})_2]^{n-}$ (M = $Mn^{II}/Cu^{II}/Zn^{II}/Cd^{II}/Ni^{II}$; X = $Ge^{IV}/P^V/Si^{IV}$),[3a,5a,7d,7e] penta-nuclear: $[Cu_5(OH)_4(H_2O)_2(A\text{-}\alpha\text{-}SiW_9O_{33})_2]^{10-}$;[3c] hexa-nuclear: $[Fe_6(OH)_3(A\text{-}\alpha\text{-}GeW_9O_{34}(OH)_3)_2]^{11-}$,[5b] $[Cu_6(en)_2(H_2O)_2(B\text{-}\alpha\text{-}GeW_9O_{34})_2]^{8-}$,[5d] $[M_6Cl_6(XW_9O_{33})_2]^{12-}$ (M = Cu^{II}/Mn^{II}; X = As^{III}/Sb^{III}),[6c] $[\{Ni_6(H_2O)_4(\mu_2\text{-}H_2O)_4(\mu_3\text{-}OH)_2\}(SiW_9O_{34})_2]^{10-}$,[8d] and $[Cu_6(enMe)_2(B\text{-}\alpha\text{-}SiW_9O_{34})_2]^{8-}$;[8f] hepta-nuclear: $[Ni_7(OH)_4(H_2O)(CO_3)_2(HCO_3)(A\text{-}\alpha\text{-}SiW_9O_{34})(\beta\text{-}SiW_{10}O_{37})]^{10-}$;[8d] and octa-nuclear: $[Cu_8(L)_4(H_2O)_2(B\text{-}\alpha\text{-}XW_9O_{34})_2]^{4-}$ (L = en/dap/2,2′-bipy; X = Ge^{IV}/Si^{IV}),[3f] and $[(A\text{-}\alpha\text{-}SiW_9O_{34})_2Co_8(OH)_6(H_2O)_2(CO_3)_3]^{16-}$.[9g]

The existence of Ge^{IV}-containing HPTs has been known for several decades, and most of the published works are based on the plenary Keggin-type germanotungstates $[GeW_{12}O_{40}]^{4-}$.[10] Since the first monolacunry germanotungstate $[GeW_{11}O_{39}]^{8-}$was reported by Hervé and Tézé in 1977,[11] lacunary germanotungstate derivatives have been discovered successively. In 1993, Liu et al. reported the trivanadium-substituted $[GeW_9V_3O_{40}]^{7-}$.[12] In 1994 Qu et al. synthesized a series of tri-TM substituted monomeric germanotungstates α-A-$[M_3(H_2O)_3GeW_9O_{37}]^{n-}$ (n = 7, M = Cr^{III}; n = 10, M = $Mn^{II}/Co^{II}/Ni^{II}/Cu^{II}$)[13] In the following year, Meng and Liu discovered the dimeric species α-$[Ga_6(H_2O)_3(GeW_9O_{37})_2]^{14-}$ and β-A-$[Ti_6O_3(GeW_9O_{37})_2]^{14-}$.[14] In 2001, a triuranium(IV)-substituted germanotungstate $[(UO)_3(GeW_9O_{34})_2]^{14-}$ was prepared by Craciun and David.[15] Kortz's group have also made some contributions to this field: in 2004, they described the synthesis, structure, and magnetic properties of the Weakley-type sandwich-type germanotungstate polyanions $[M_4(H_2O)_2(\alpha\text{-}B\text{-}GeW_9O_{34})_2]^{12-}$ (M = $Mn^{II}/Cu^{II}/Zn^{II}/Cd^{II}$);[5a] subsequently, other novel germanotungstates such as $[Fe_6(OH)_3(\alpha\text{-}A\text{-}GeW_9O_{34}(OH)_3)_2]^{11-}$,[5b] $[(RuC_6H_6)_2GeW_9O_{34}]^{6-}$,[16] $[\gamma\text{-}GeW_{10}O_{36}]^{8-}$,[17] $[\{Ru(C_6H_6)(H_2O)\}\{Ru(C_6H_6)\}(\gamma\text{-}GeW_{10}O_{36})]^{4-}$,[18a] $[K(H_2O)(\beta\text{-}Fe_2GeW_{10}O_{37}(OH))(\gamma\text{-}GeW_{10}O_{36})]^{12-}$, and $[\{\beta\text{-}Fe_2GeW_{10}O_{37}(OH)_2\}_2]^{12-}$[18b] were reported by them; in 2007, they communicated an unprecedented 20-Ce^{III} containing tungstogermanate $[Ce_{20}Ge_{10}W_{100}O_{376}(OH)_4(H_2O)_{30}]^{56-}$, which can be described as a dimeric entity composed of two units of $[Ce_{10}Ge_5W_{50}O_{188}(OH)_2(H_2O)_{15}]^{28-}$ linked together through Ce−O(W) bridges.[19] Very recently, Wang et al. reported a high-nuclear copper-substituted germanotungstate $K_{10}Na_{14}[Cu_{10}(H_2O)_2(N_3)_4(\alpha\text{-}B\text{-}GeW_9O_{34})_2(\beta\text{-}B\text{-}GeW_8O_{31})_2]\cdot 30H_2O$,[20] in which two $[\beta\text{-}B\text{-}GeW_8O_{31}]^{10-}$ units and two $[\alpha\text{-}B\text{-}GeW_9O_{34}]^{10-}$ units are connected together by a $[Cu_{10}(N_3)_4O_{32}(H_2O)_2]$ cluster to construct a tetrameric structure. In addition, in the past 2 years, Yang et al. reported several inorganic−organic TM-substituted germanotungstates.[3e,3f,5c,5d,21] Our lab has also made some work in the germanotungstate field.[22]

(7) (a) Wang, J. P.; Ma, P. T.; Shen, Y.; Niu, J. Y. *Cryst. Growth Des.* **2007**, 603. (b) Weakley, T. J. R.; Finke, R. G. *Inorg. Chem.* **1990**, *29*, 1235. (c) Tourné, C. M.; Tourné, G. F.; Zonnevijlle, F. *J. Chem. Soc., Dalton Trans.* **1991**, 143. (d) Casañ-Pastor, N.; Bas-Serra, J.; Coronado, E.; Pourroy, G.; Baker, L. C. W. *J. Am. Chem. Soc.* **1992**, *114*, 10380. (e) Clemente-Juan, J. M.; Coronado, E.; Galán-Mascarós, J. R.; Gómez-García, C. J. *Inorg. Chem.* **1999**, *38*, 55. (f) Finke, R. G.; Weakley, T. J. R. *J. Chem. Crystallogr.* **1994**, *24*, 123. (g) Kirby, J. F.; Baker, L. C. W. *J. Am. Chem. Soc.* **1995**, *117*, 10010. (h) Crano, N. J.; Chambers, R. C.; Lunch, V. M.; Fox, M. A. *J. Mol. Catal. A.* **1996**, *114*, 65. (i) Zhang, X.; Duncan, D. C.; Campana, C. F.; Hill, C. L. *Inorg. Chem.* **1997**, *36*, 4208. (j) Müller, A.; Peter, F.; Pope, M. T.; Gatteschi, D. *Chem. Rev.* **1998**, *98*, 239. (k) Song, W.; Wang, X.; Liu, Y.; Liu, J.; Xu, H. *J. Electroanal. Chem.* **1999**, *479*, 85. (l) Gómez-García, C. J.; Borrás-Almenar, J. J.; Coronado, E.; Ouahab, L. *Inorg. Chem.* **1994**, *33*, 4016. (m) Finke, R. G.; Rapko, B.; Weakley, T. J. R. *Inorg. Chem.* **1989**, *28*, 1573.

(8) (a) Kato, C. N.; Shinohara, A.; Hayashi, K.; Nomiya, K. *Inorg. Chem.* **2006**, *45*, 8108. (b) Bassil, B. S.; Dickman, M. H.; Kortz, U. *Inorg. Chem.* **2006**, *45*, 2394. (c) Yamase, T.; Fukaya, K.; Nojiri, H.; Ohshima, Y. *Inorg. Chem.* **2006**, *45*, 7698. (d) Zhang, Z. M.; Li, Y. G.; Wang, E. B.; Wang, X. L.; Qin, C.; An, H. Y. *Inorg. Chem.* **2006**, *45*, 4313. (e) Zhang, Z. M.; Qi, Y. F.; Qin, C.; Li, Y. G.; Wang, E. B.; Wang, X. L.; Su, Z. M.; Xu, L. *Inorg. Chem.* **2007**, *46*, 8162. (f) Zheng, S. T.; Yuan, D. Q.; Zhang, J.; Yang, G. Y. *Inorg. Chem.* **2007**, *46*, 4569. (g) Ruhlmann, L.; Canny, J.; Contant, R.; Thouvenot, R. *Inorg. Chem.* **2002**, *41*, 3811. (h) Zhang, X.; Anderson, T. M.; Chen, Q.; Hill, C. L. *Inorg. Chem.* **2001**, *40*, 418. (i) Andres, H.; Clemente-Juan, J. M.; Basler, R.; Aebersold, M.; Güdel, H.-U.; Borrás-Almenar, J. J.; Gaita-Ariño, A.; Coronado, E.; Büttner, H.; Janssen, S. *Inorg. Chem.* **2001**, *40*, 1943. (j) Anderson, T. M.; Hardcastle, K. I.; Okun, N.; Hill, C. L. *Inorg. Chem.* **2001**, *40*, 6418. (k) Anderson, T. M.; Zhang, X.; Hardcastle, K. I.; Hill, C. L. *Inorg. Chem.* **2002**, *41*, 2477. (l) Limanski, E. M.; Piepenbrink, M.; Droste, E.; Burgemeister, K.; Krebs, B. *J. Cluster Sci.* **2002**, *13*, 369.

(9) (a) Mbomekalle, I. M.; Keita, B.; Nadjo, L.; Hardcastle, K. I.; Hill, C. L.; Anderson, T. M. *Dalton Trans.* **2004**, 4094. (b) Ritorto, M. D.; Anderson, T. M.; Neiwert, W. A.; Hill, C. L. *Inorg. Chem.* **2004**, *43*, 44. (c) Stowe, A. C.; Nellutla, S.; Dalal, N. S.; Kortz, U. *Eur. J. Inorg. Chem.* **2004**, 3792. (d) Clemente-Juan, J. M.; Coronade, E.; Forment-Aliaga, A.; Galán-Mascarós, J. R.; Giménez-Saiz, C.; Gómez-García, C. J. *Inorg. Chem.* **2004**, *43*, 2689. (e) Nellutla, S.; Tol, J. V.; Dalal, N. S.; Bi, L. H.; Kortz, U.; Keita, B.; Nadjo, L.; Khitrov, G. A.; Marshall, A. G. *Inorg. Chem.* **2005**, *44*, 9795. (f) Bassil, B. S.; Kortz, U.; Tigan, A. S.; Clemente-Juan, J. M.; Keita, B.; Oliveira, P. D.; Nadjo, L. *Inorg. Chem.* **2005**, *44*, 9360. (g) Lisnard, L.; Mialane, P.; Dolbecq, A.; Marrot, J.; Clemente-Juan, J. M.; Coronado, E.; Keita, B.; Oliveira, P. D.; Nadjo, L.; Sécheresse, F. *Chem.—Eur. J.* **2007**, *13*, 3525. (h) Ruhlmann, L.; Nadjo, L.; Canny, J.; Contant, R.; Thouvenot, R. *Eur. J. Inorg. Chem.* **2002**, 975. (i) Mbbomekalle, I. M.; Keita, B.; Nierlich, M.; Kortz, U.; Berthet, P.; Nadjo, L. *Inorg. Chem.* **2003**, *42*, 5143. (j) Fang, X. K.; Anderson, T. M.; Neiwert, W. A.; Hill, C. L. *Inorg. Chem.* **2003**, *42*, 8600. (k) Limanski, E. M.; Drewes, D.; Droste, E.; Böhner, R.; Krebs, B. *J. Mol. Struct.* **2003**, *656*, 17. (l) Gaunt, A. J.; May, I.; Copping, R.; Bhatt, A. I.; Collison, D.; Fox, O. D.; Holman, K. T.; Pope, M. T. *Dalton Trans.* **2003**, 3009. (m) Mbomekalle, I. M.; Keita, B.; Nadjo, L.; Berthet, P.; Neiwert, W. A.; Hill, C. L.; Ritorto, M. D.; Anderson, T. M. *Dalton Trans.* **2003**, 2646.

(10) (a) Katano, H.; Osakai, T.; Himeno, S.; Saito, A. *Electrochim. Acta* **1995**, *40*, 2935. (b) Wilde, W.; Backer, C.; Lunk, H. J. *Z. Chem.* **1989**, *29*, 346. (c) Dorokhova, E. N.; Kazanskii, L. P.; Prokhorova, G. V. *Zh. Neorg. Khim.* **1985**, *30*, 2795. (d) Biquard, M.; Souchay, P. *Ann. Chim. Paris.* **1975**, *10*, 163. (e) Biquard, M. *C. R. Acad. Sci. Ser. C* **1975**, *281*, 309. (f) Leyrie, M.; Herve, G. *C. R. Acad. Sci. Ser. C* **1973**, *276*, 911. (g) Biquard, M.; Lamache, M. *Bull. Soc. Chim. France* **1971**, *1*, 32.

(11) Hervé, G.; Tézé, A. *Inorg. Chem.* **1977**, *16*, 2115.

(12) Liu, J. F.; Zhao, B. L.; Rong, C. Y.; Pope, M. T. *Acta Chim. Sin.* **1993**, *51*, 368.

(13) Qu, L. Y.; Sun, Y. J.; Chen, Y. G.; Yu, M.; Peng, J. *Synth. React. Inorg. Met.-Org. Chem.* **1994**, *24*, 1339.

(14) (a) Meng, L.; Liu, J. F. *Chin. J. Chem.* **1995**, *13*, 334. (b) Meng, L.; Liu, J. F. *Chin. Chem. Lett.* **1995**, *6*, 265.

(15) Craciun, C.; David, L. *J. Alloys Compd.* **2001**, *323*−*324*, 743.

(16) Bi, L. H.; Kortz, U.; Dickman, M. H.; Keita, B.; Nadjo, L. *Inorg. Chem.* **2005**, *44*, 7485.

(17) Nsouli, N. H.; Bassil, B. S.; Dickman, M. H.; Kortz, U.; Keita, B.; Nadjo, L. *Inorg. Chem.* **2006**, *45*, 3858.

(18) (a) Bi, L. H.; Chubarova, E. V.; Nsouli, N. H.; Dickman, M. H.; Kortz, U.; Keita, B.; Nadjo, L. *Inorg. Chem.* **2006**, *45*, 8575. (b) Nsouli, N. H.; Mal, S. S.; Dickman, M. H.; Kortz, U.; Keita, B.; Nadjo, L.; Clemente-Juan, J. M. *Inorg. Chem.* **2007**, *46*, 8763.

(19) Bassil, B. S.; Dickman, M. H.; Römer, I.; Kammer, B. V. D.; Kortz, U. *Angew. Chem., Int. Ed.* **2007**, *46*, 6192.

(20) Zhang, Z. M.; Qi, Y. F.; Qin, C.; Li, Y. G.; Wang, E. B.; Wang, X. L.; Su, Z. M.; Xu, L. *Inorg. Chem.* **2007**, *46*, 8162.

(21) Wang, C. M.; Zheng, S. T.; Yang, G. Y. *Inorg. Chem.* **2007**, *46*, 616.

More than 10 years ago, sandwich-type HPMs $[Nd(GeMo_{11}O_{39})_2]^{13-}$ and $[Dy(SiMo_{11}O_{39})_2]^{13-}$ based on monovacant Keggin polyoxoanions were reported.[23] Later, the May group extended this study to the $[Ln(PMo_{11}O_{39})_2]^{11-}$ system.[24,25]

Compared with monovacant Keggin HPMs, the reports on sandwich-type HPMs based on trivacant Keggin units are very limited.[26,27] Recently, Xu et al. addressed two di-TM sandwiched arsenomolybdate and vanadiummolybdate.[27] However, no tetra-TM sandwiched HPM analogue has been reported. Why have only few sandwich-type HPMs been reported so far? The main reasons are as follows: First, it is very difficult to prepare trivacant HPM precursors probably because trivacant HPM polyoxoanions are labile and very easy to rearrange into a saturated or monovacant Keggin polyoxoanions; therefore, the successful isolation of trivacant HPM polyoxoanions still remains a great challenge; Second, in recent years, very few people concentrate on the study of HPMs. In this context, we have spent much time and attention on this field with the aim of finding rational reaction conditions to obtain novel TM-substituted sandwich-type HPMs. In our experiments, the simple starting materials were utilized in stoichiometric amounts rather than trivacant HPM precursors. Finally, five novel TM-substituted sandwich-type germanomolybdates were separated, which were formulated as $Na_{12}(H_2O)_{36}[Cu_2(\beta\text{-Y-}GeMo_9O_{33})_2]\cdot 3H_2O$ (**1**), $[N(CH_3)_4]_4[Na_6(H_2O)_{24}][Cr_2((\beta\text{-Y-}GeMo_9O_{33})_2]\cdot 7H_2O$ (**2**), and $[Na_{11}(H_2O)_{25}]H[M_4(H_2O)_2(\alpha\text{-B-}GeMo_9O_{34})_2]\cdot 6H_2O$ (M = Ni^{II} for **3**, M = Mn^{II} for **4**, and M = Co^{II} for **5**). To the best of our knowledge, **1**−**5** are the first sandwich-type germanomolybdates containing both $\{\beta\text{-X-}GeMo_9O_{33}\}/\{\alpha\text{-B-}GeMo_9O_{34}\}$ fragments and TM cations. It is interesting that **1** and **2** display the rare dinuclear TM-substituted sandwich-type structures with unusual β-Y-type germanomolybdate units whereas **3**−**5** exhibit the first tetranuclear TM-substituted sandwich-type structures with familiar α-B-type germanomolybdate units.

Experimental Section

General Methods and Materials. All reagents were used as purchased without further purification. Elemental analyses (C, H, and N) were performed on a Perkin-Elmer 240C elemental analyzer. Inductively coupled plasma (ICP) spectra were performed on a Perkin-Elmer Optima 2000 ICP-OES spectrometer. IR spectra were obtained from a solid sample palletized with KBr on Nicolet 170 SXFT-IR spectrometer in the range 400−4000 cm^{-1}. UV absorption spectra were obtained with a U-4100 spectrometer at room temperature. XPS were recorded on an Axis Ultra (Kratos, U.K.) photoelectron spectroscope using monochromatic Al Kα (1486.7 eV) radiation. Thermogravimetric analyses were performed in N_2 on a Perkin-Elmer-7 instrument with a heating rate of 10 °C/min. XRPD measurements were performed on a Philips X'Pert-MPD instrument with Cu Kα radiation (λ = 1.54056 Å) in the angular range 2θ = 10−40° at 293 K. Surface photovoltage spectroscopy (SPS) and electric field induced SPS (EFISPS) were carried out on a Lock-in based surface photovoltage measurement system which was constituted of a source of monochromatic light, a lock-in amplifier (SR830-DSP) with a light chopper (SR540), a sample cell, and a computer. A low chopping frequency of ∼46 Hz was used. Magnetic susceptibility measurements were obtained by the use of a Quantum Design MPMS-XL7 SQUID magnetometer at a temperature ranging from 2 to 300 K.

Preparation of $[Na_{12}(H_2O)_{36}][Cu_2(\beta\text{-Y-}GeMo_9O_{33})_2]\cdot 3H_2O$ (1). $Na_2MoO_4\cdot 2H_2O$ (2.08 g, 8.60 mmol) and GeO_2 (0.10 g, 0.96 mmol) were successively dissolved in 40 mL of HAc-NaAc buffer solution (pH = 4.8, 0.5 $mol\cdot L^{-1}$), and then $Cu(Ac)_2\cdot H_2O$ (0.38 g, 1.92 mmol) was added. The resulting mixture was heated in water bath (80 °C) for 2 h and filtered after cooling. Slow evaporation at room temperature led to green crystals suitable for X-ray diffraction within 1−2 weeks, which were collected by filtration and dried in air (Yield: ca. 60% based on Mo). Elemental analyses calcd (%) for $H_{78}Cu_2Ge_2Mo_{18}Na_{12}O_{105}$: H, 1.95; Na, 6.84; Cu, 3.15; Ge, 3.60; Mo, 42.81; found: H, 1.81; Na, 6.77; Cu, 3.29; Ge, 3.49; Mo, 42.72. IR (KBr pellets, v/cm^{-1}, Supporting Information, Figure S1): 1634 (s), 1383 (w), 930 (m), 890 (s), 766 (s), 691 (m), 523 (w), 413 (m).

Preparation of $[N(CH_3)_4]_4[Na_6(H_2O)_{24}][Cr_2(\beta\text{-Y-}GeMo_9O_{33})_2]\cdot 7H_2O$ (2). The preparation of **2** was similar to that of **1**, except that $CrCl_3\cdot 6H_2O$ (0.51 g, 1.92 mmol) replaced $Cu(Ac)_2\cdot H_2O$. Additionally, tetramethylammonium bromide (0.10 g, 0.65 mmol) was added after cooling. Slow evaporation at room temperature afforded purple red crystals suitable for X-ray diffraction after 1−2 weeks, which were collected by filtration and dried in air (Yield: ca. 13% based on Mo). Elemental analyses calcd (%) for $C_{16}H_{110}N_4Cr_2Ge_2Mo_{18}Na_6O_{97}$: C, 4.77; H, 2.75; N, 1.39; Na, 3.43; Cr, 2.58; Ge, 3.61; Mo, 42.90; found: C, 4.68; H, 2.62; N, 1.44; Na, 3.39; Cr, 2.67; Ge, 3.74; Mo, 42.85. IR (KBr pellets, v/cm^{-1}, Supporting Information, Figure S1): 1629 (s), 1482 (s), 933 (m), 873 (s), 764 (s), 686 (s), 528 (w), 418 (m).

Preparation of $[Na_{11}(H_2O)_{25}]H[Ni_4(H_2O)_2(\alpha\text{-B-}GeMo_9O_{34})_2]\cdot 6H_2O$ (3). The preparation of **3** was similar to that of **1**, except that $Ni(Ac)_2\cdot 4H_2O$ (0.48 g, 1.92 mmol) replaced $Cu(Ac)_2\cdot H_2O$. Slow evaporation at room temperature resulted in yellow crystals suitable for X-ray diffraction within 1−2 weeks, which were collected by filtration and dried in air (Yield: ca. 30% based on Mo). Elemental analyses calcd (%) for $H_{66}Ni_4Ge_2Mo_{18}Na_{11}O_{101}$: H, 1.65; Na, 6.26; Ni, 5.81; Ge, 3.59; Mo, 42.72; found: H, 1.52; Na, 6.35; Ni, 5.72; Ge, 3.50; Mo, 42.61. IR (KBr pellets, v/cm^{-1}, Supporting Information, Figure S2): 1620 (s), 1378 (w), 924 (m), 875 (s), 771 (s), 722 (w), 591 (w), 465 (m).

Preparation of $[Na_{11}(H_2O)_{25}]H[Mn_4(H_2O)_2(\alpha\text{-B-}GeMo_9O_{34})_2]\cdot 6H_2O$ (4). A buffer layer of the ethanol/water (2:2, v/v) solution (4 mL) was carefully layered onto a HAc-NaAc solution (4 mL) containing $Na_2MoO_4\cdot 2H_2O$ (0.52 g, 2.15 mmol) and GeO_2 (0.25 g, 0.24 mmol) in a test tube. Then, an HAc-NaAc solution (4 mL) containing $Mn(Ac)_2\cdot 6H_2O$ (0.1 g, 0.36 mmol) was carefully layered onto the buffer layer. Rufous crystals appeared after 5−6 months, and were collected and dried in air (Yield: ca. 10% based on Mo). Elemental analyses calcd (%) for $H_{66}Mn_4Ge_2Mo_{18}Na_{11}O_{101}$: H, 1.65; Na, 6.28; Mn, 5.46; Ge, 3.61; Mo, 42.88; found: H, 1.78; Na, 6.15; Mn, 5.55; Ge, 3.73; Mo, 42.81. IR (KBr pellets, v/cm^{-1}, Supporting

(22) (a) Wang, J. P.; Zhao, J. W.; Duan, X. Y.; Niu, J. Y. *Cryst. Growth Des.* **2006**, 507. (b) Wang, J. P.; Duan, X. Y.; Du, X. D.; Niu, J. Y. *Cryst. Growth Des.* **2006**, 2266. (c) Wang, J. P.; Du, J.; Niu, J. Y. *CrystEngComm.* **2008**, *10*, 972. (d) Wang, J. P.; Ma, P. T.; Shen, Y.; Niu, J. Y. *Cryst. Growth Des.* **2008**, 3130.

(23) (a) Shan, Y. K.; Liu, Z. X.; Wang, B. E.; Jin, Z. S.; Wei, G. C.; Liu, Y. S. *Chinese J. Struct. Chem.* **1990**, *9*, 159. (b) Wang, E. B.; Shan, Y. K.; Zu, Z. X.; Liu, J. F.; Zhang, B. G. *Acta. Chim. Sin.* **1991**, *49*, 774. (c) Shan, Y. K.; Liu, Z. X.; Jin, Z. S.; Wei, G. C. *Acta. Chim. Sin.* **1992**, *50*, 357.

(24) Copping, R.; Jonasson, L.; Gaunt, A. J.; Drennan, D.; Collison, D.; Helliwell, M.; Pirttijarvi, R. J.; Jones, C. J.; Huguet, A.; Apperley, D. C.; Kaltsoyannis, N.; May, I. *Inorg. Chem.* **2008**, *47*, 5787.

(25) (a) Gaunt, A. J.; May, I.; Sarsfield, M. J.; Collison, D.; Helliwell, M.; Dennis, I. S. *Dalton Trans.* **2003**, 2767. (b) Copping, R.; Gaunt, A. J.; May, I.; Sarsfield, M. J.; Collison, D.; Helliwell, M.; Dennis, I. S.; Apperley, D. C. *Dalton Trans.* **2005**, 1256.

(26) Fukushima, H. F.; Kobayashi, A.; Sasaki, Y. *Acta Crystallogr., Sect. B: Struct. Sci.* **1981**, *37*, 1613.

(27) (a) Yang, Y. Y.; Xu, L.; Gao, G. G.; Li, F. Y.; Qiu, Y. F.; Qu, X. S.; Liu, H. *Eur. J. Inorg. Chem.* **2007**, 2500. (b) Yang, Y. Y.; Xu, L.; Gao, G. G.; Li, F. Y.; Liu, X. Z.; Guo, W. H. *Eur. J. Inorg. Chem.* **2009**, 1460.

Table 1. Crystallographic Data and Structural Refinements for **1**−**5**

	1	2	3	4	5
empirical formula	$H_{78}Cu_2Ge_2Mo_{18}Na_{12}O_{105}$	$C_{16}H_{110}N_4Cr_2Ge_2Mo_{18}Na_6O_{97}$	$H_{66}Ni_4Ge_2Mo_{18}Na_{11}O_{101}$	$H_{66}Mn_4Ge_2Mo_{18}Na_{11}O_{101}$	$H_{66}Co_4Ge_2Mo_{18}Na_{11}O_{101}$
formula weight	4033.68	4025.12	4042.36	4027.28	4043.28
crystal system	triclinic	triclinic	triclinic	triclinic	triclinic
space group	$P\bar{1}$	$P\bar{1}$	$P\bar{1}$	$P\bar{1}$	$P\bar{1}$
a/Å	13.2369(8)	13.3571(12)	11.6135(8)	11.6756(10)	11.584(3)
b/Å	13.5286(8)	13.5019(12)	12.8737(9)	12.9056(11)	12.856(4)
c/Å	16.6405(13)	18.4660(17)	17.1160(17)	17.3437(15)	17.173(7)
α/deg	73.2850(10)	76.9310(10)	97.3750(10)	97.3770(2)	97.380(6)
β/deg	66.56	77.5830(10)	107.005(10)	106.8390(10)	106.906(6)
γ/deg	60.71	61.0300(10)	111.624(10)	111.8450(10)	111.713(4)
V/Å^3	2368.4(3)	2816.3(4)	2193.2(3)	2238.1(3)	2191.7(13)
Z	1	1	1	1	1
T/K	293(2)	293(2)	293(2)	293(2)	293(2)
ρ_{calc}/g·cm^{-3}	2.828	2.373	3.061	2.988	3.063
μ/mm^{-1}	3.546	2.773	4.178	3.817	4.079
data/parameters	8059/632	9841/670	7573/628	7797/628	7642/628
GOF	1.076	1.050	1.087	1.045	1.035
R_1 [$I > 2\sigma(I)$]	0.0327	0.0249	0.0332	0.0547	0.0601
wR_2	0.0862	0.0745	0.0911	0.1338	0.1672

Information, Figure S2): 1619 (s), 1380 (w), 928 (s), 864 (s), 762 (s), 718 (w), 596 (w), 450 (m).

Preparation of $[Na_{11}(H_2O)_{25}]H[Co_4(H_2O)_2(\alpha\text{-B-}GeMo_9O_{34})_2]\cdot 6H_2O$ (5). The preparation of **5** was similar to that of **4**, except that $Co(Ac)_2\cdot 6H_2O$ (0.1 g, 0.35 mmol) replaced $Mn(Ac)_2\cdot H_2O$. Red crystals appeared after 4−5 months and were collected and dried in air (Yield: ca. 16% based on Mo). Elemental analyses calcd (%) for $H_{66}Co_4Ge_2Mo_{18}Na_{11}O_{101}$: H, 1.64; Na, 6.25; Co, 5.83; Ge, 3.59; Mo, 42.71; found: H, 1.58; Na, 6.31; Co, 5.74; Ge, 3.66; Mo, 42.65. IR (KBr pellets, v/cm^{-1}, Supporting Information, Figure S2): 1621 (s), 1382 (W), 924 (s), 866 (s), 770 (s), 724 (w), 608 (w), 453 (m).

X-ray Crystallography. Intensity data for **1**−**5** were collected on Bruker CCD Apex-II diffractometer with Mo Kα radiation (λ = 0.71073 Å) at 293K. The structures of **1**−**5** were resolved by direct methods using the SHELXTL-97 program package.[28] The remaining atoms were found from successive full-matrix least-squares refinements on F^2 and Fourier syntheses. Lorentz polarization and empirical absorption corrections were applied. No hydrogen atoms associated with the water molecules were located from the difference Fourier map. Positions of the hydrogen atoms attached to the carbon and nitrogen atoms were geometrically placed. All hydrogen atoms were refined isotropically as a riding mode using the default SHELXTL parameters. Crystallographic data and structural refinements for **1**−**5** are summarized in Table 1. Absorption effects were empirically applied. CSD reference no. 419901, 419902, 420542, and 420723 for **1**, **3**, **4** and **5**, respectively and CCDC reference no. 702821 for **2**. Further details on the crystal structure investigations of **1**, **3**, **4**, and **5** may be obtained from the Fachinformationszentrum Karlsruhe, 76344 Eggenstein-Leopoldshafen, Germany (fax:(+49) 7247−808−666; e-mail: crysdata@fiz-karlsruhe.de). The data of **2** can be obtained free of charge from The Cambridge Crystallographic Data Centre via www.ccdc.cam.ac.uk/data_ request/cif.

Results and Discussion

Synthesis, IR, UV, and XPS Spectra. In comparison with lacunary HPT polyoxoanions, lacunary HPM polyoxoanions generally show more structural lability in aqueous solution,[24,27] as a result, it is rather difficult to isolate di/trivacant lacunary HPM polyoxoanions and their sandwich-type species. In this paper, we developed a rational one-pot synthetic strategy to prepare sandwich-type HPM species. **1** was synthesized with a high yield (60%) in HAc-NaAc solution by direct reaction of $Na_2MoO_4\cdot 2H_2O$, GeO_2, and $Cu(Ac)_2\cdot H_2O$. When we prepared **2**, tetramethylammonium bromide was used; moreover, the yield of **2** was low (13%). In contrast, without addition of tetramethylammonium bromide, only powder was formed. The comparison between the IR spectrum of powder and that of **2** suggests that powder should be di-Cr^{III} substituted sandwich-type germanomolybdate containing trivacant {β-Y-$GeMo_9O_{33}$} units (Supporting Information, Figure S3 and Table S1). So, we presume that tetramethylammonium bromide in the preparation of **2** is beneficial for the growth of good crystals of **2**. Such a phenomenon that organic amine cations (tetramethyl-ammonium, hexamethylenetetraamine, triethanolammonium) can kinetically stabilize and help the improved crystallization has been previously encountered.[29] Yellow crystals of **3** with a high yield (30%) were prepared using a similar method to **1** except that Ni^{II} replaced Cu^{II}. When we attempted to obtain other first-row TM-substituted sandwich-type germanomolybdates, this strategy failed. Therefore, we had to change our strategy to synthesize other first-row TM-substituted sandwich-type germanomolybdates. At last, we found that the diffused method can prepare **4** and **5**. The diffusion of the HAc-NaAc solution containing $Mn(Ac)_2\cdot 6H_2O$/$Co(Ac)_2\cdot 6H_2O$ into the HAc-NaAc solution including $Na_2MoO_4\cdot 2H_2O$ and GeO_2 by means of the buffer layer of the ethanol/water resulted in crystals of **4** and **5**, but their yields were very low. The further work with the aim of enhancing the yield is still in progress. In addition, persistent attempts to isolate tetra-Cu^{II}/Cr^{III}-substituted and di-Ni^{II}/Mn^{II}/ Co^{II}-substituted sandwich-type germanomolybdates by changing reaction conditions such as temperatures, pH values of buffer solution,

(28) (a) Sheldrick, G. M. *SHELXL 97, Version 5.1, Program for Crystal Structure Solution and Refinement*; University of Göttingen: Göttingen, Germany, 1997. (b) Sheldrick, G. M. *SADABS, Program for Empirical Absorption Correction of Area Detector Data*; University of Göttingen, Göttingen, Germany, 1996.

(29) Long, D. L.; Song, Y. F.; Wilson, E. F.; Kögerler, P.; Guo, S. X.; Bond, A. M.; Hargreaves, J. S. J.; Cronin, L. *Angew. Chem., Int. Ed.* **2008**, *47*, 4384.

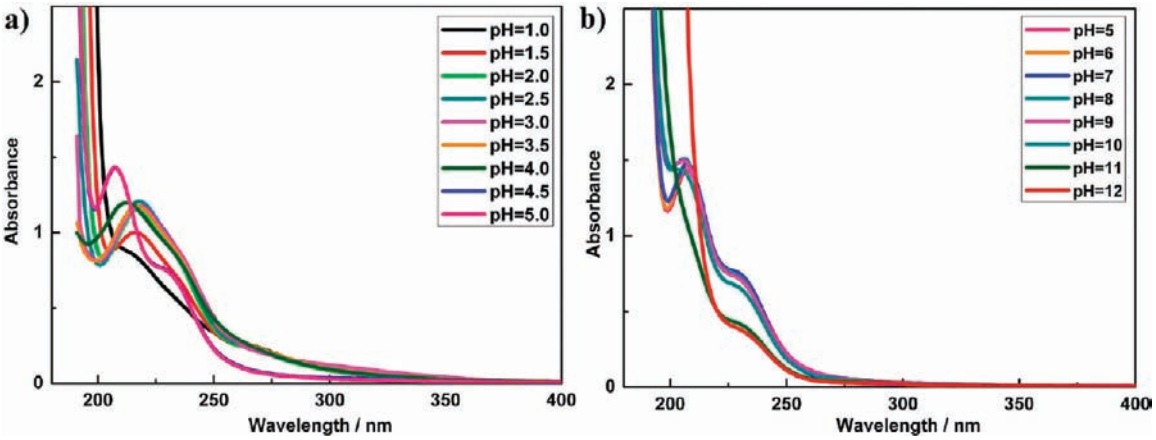

Figure 1. Influence of the pH values on the stability of **1** in aqueous solution: (a) The UV spectral evolution in acidic direction; (b) The UV spectral evolution in alkaline direction.

and ratios of starting materials were unsuccessful. These results suggest that the nature of the TM ions plays an important role in the formation of the two structural types.

Four points can be concluded from the successful syntheses of **1**−**5**: (a) Sodium acetate buffer solution may be favorable to the formation of lacunary germanomolybdate units in aqueous solution, and the optimum pH range of buffer solution is 4.5−5.0; (b) The incorporation of TM cations in the sandwich belt can enhance the stability of lacunary germanomolybdate units; (c) The heating condition is improved by mild water-bath heating instead of direct heating, and the results show that the most appropriate temperatures vary from 70 to 90 °C; (d) The nature of the TM ions can influence the structural type. In addition, **1**−**5** are obtained directly from the reaction of the simple materials in stoichiometric amounts, which shows that lacunary HPM precursors are not necessary for the syntheses of TM-substituted sandwich-type HPM species under appropriate reaction conditions. In a word, the rational one-pot synthetic strategy developed by us in the paper can shorten the preparation process of TM-substituted sandwich-type HPM species in comparison with that by means of lacunary HPM precursors.

The peak shapes of the IR spectra in the 400−1000 cm^{-1} region of **1** and **2** are similar while those of **3**−**5** are similar (Supporting Information, Figures S1, S2), indicating the structural type of the polyoxoanions in **1** and **2** is almost the same, and that in **3**−**5** is also isostructural, which are in good agreement with the results of X-ray diffraction structural analyses. In the low-wavenumber region, characteristic vibration patterns derived from the Keggin frameworks are observed. Four characteristic bands assigned to $\nu(Mo-O_t)$, $\nu(Ge-O_a)$, $\nu(Mo-O_b)$, and $\nu(Mo-O_c)$ appear at 930, 890, 766, and 691 cm^{-1} for **1**; 933, 873, 764, and 686 cm^{-1} for **2**; 924, 875, 771, and 722 cm^{-1} for **3**; 928, 864, 762, and 718 cm^{-1} for **4**; 924, 866, 770, and 724 cm^{-1} for **5**, respectively.[5c] Additionally, the presence of $[N(CH_3)_4]^+$ in **2** is suggested by the occurrence of the apparent vibrational band centered at 1482 cm^{-1}.

The UV spectra of **1**−**5** in aqueous solution all display two similar absorption peaks (Supporting Information, Figure S4) at 208 and 233 nm for **1**, 207 and 238 nm for **2**, 206 and 232 nm for **3**, 207 and 233 nm for **4**, 205 and 233 for **5**, respectively. The higher energy spectral band can be assigned to the charge transfer transitions of the $O_t \rightarrow Mo$ band, whereas the lower one can be attributed to those of the $O_{b,c} \rightarrow Mo$ band, suggesting the presence of polyoxoanions. In comparison with the aqueous solution UV spectra of **1** and **3**, the two spectral bands (at 209 and 237 nm for **1**, 211 and 236 nm for **3**) of the solid state UV spectra of **1** and **3** (Supporting Information, Figure S5) have almost no obvious shift, indicating that the polyoxoanion skeletons of **1** and **3** still are retained in aqueous solution.

To investigate the influences of the pH value on the stability of compounds in aqueous solution, in situ UV spectroscopic measurements of **1** and **3** were performed in aqueous solution. The pH values in the acidic direction were adjusted using diluted HCl solution while the pH values in the alkaline direction were adjusted using diluted NaOH solution. The pH value of **1** that was dissolved in water (2×10^{-4} mol·L^{-1}) was 5.0, and the pH value of **3** that was dissolved in water (4×10^{-4} mol·L^{-1}) was 6.0. As is shown in Figure 1a, the UV spectra of **1** in aqueous solution display two absorption bands at about 208 and 233 nm at pH = 5.0; when the pH value gradually decreases near 4.5, the change of the two absorption bands is not obvious. With the pH value further decreasing, the absorption band at 208 nm is gradually red-shifted; meanwhile the absorption band at 233 nm slowly disappears. The reason for the red-shift of the $O_t \rightarrow Mo$ band may be related to the protonation of the terminal oxygen atoms of polyoxoanions. A conclusion can be drawn that the skeleton of **1** has been destroyed at the pH lower than 4.5. In contrast, when the pH value of **1** increases (Figure 1b), the absorption band at 208 nm is more and more weak until it vanishes whereas the solution absorbance becomes larger, indicating that the $[Cu_2(\beta\text{-Y-GeMo}_9O_{33})_2]^{12-}$ polyoxoanions may be gradually decomposed to MoO_4^{2-} ions, which are also explained by the UV spectrum of $Na_2MoO_4 \cdot 2H_2O$ (Supporting Information, Figure S6); at the same time, the absorption band at 233 nm is more and more weak until it withers away, suggesting the decomposition of skeleton of **1**. The above analyses show

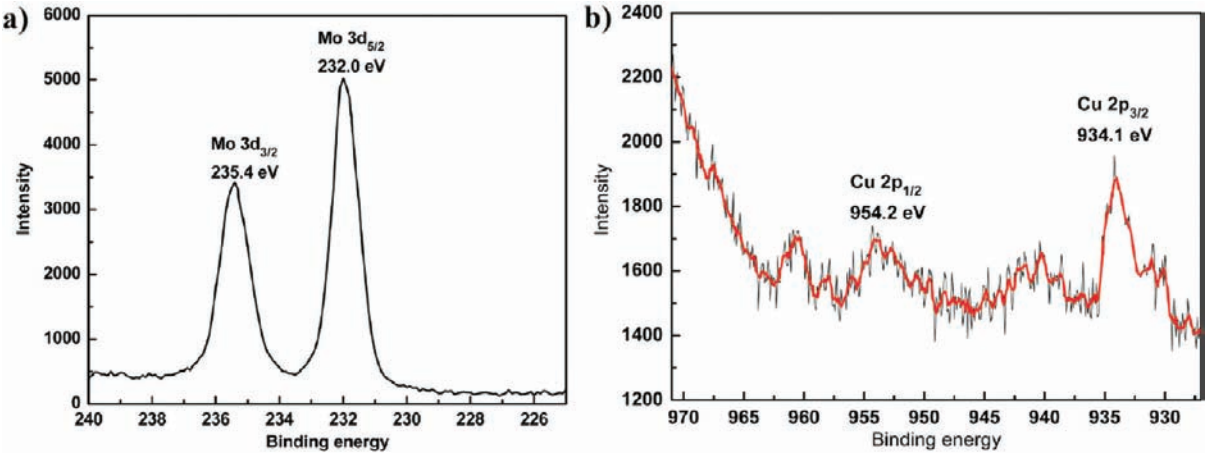

Figure 2. (a) XPS spectra of **1** for Mo $3d_{5/2}$ and Mo$3d_{3/2}$; (b) XPS spectra of **1** for Cu $2p_{3/2}$ and Cu $2p_{1/2}$.

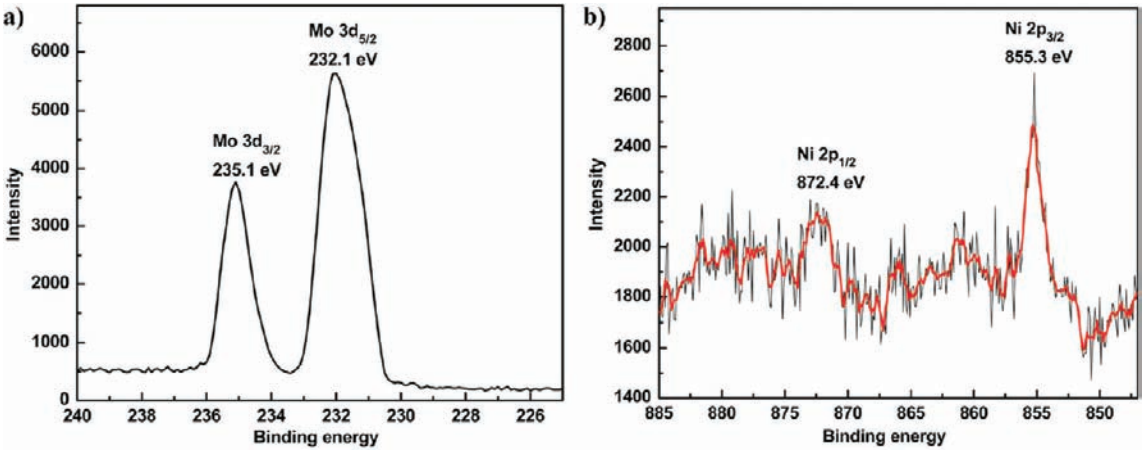

Figure 3. (a) XPS spectra of **3** for Mo $3d_{5/2}$ and Mo$3d_{3/2}$; (b) XPS spectra of **3** for Ni $2p_{3/2}$ and Ni $2p_{1/2}$.

that the pH stable ranges of aqueous solution of **1** are about 4.5−10. For **3**, the influences of the pH value on the stability of **3** in aqueous solution are similar to those of **1** (Supporting Information, Figure S7). The pH stable ranges of aqueous solution of **3** are about 3.0−10.

The bond valence sum (BVS) calculations[30a] of **1** and **3** indicate that the oxidation states of all Mo and Cu atoms in **1** are +6 and +2 respectively, and the oxidation states of all Mo and Ni atoms in **3** are +6 and +2 respectively, which are further confirmed by XPS spectra. For **1** (Figure 2), the XPS spectra exhibit two overlapped peaks at 232.0 and 235.4 eV, attributing to Mo^{6+} ($3d_{5/2}$) and Mo^{6+} ($3d_{3/2}$)[30b,c] respectively; and two peaks at 934.1 and 954.2 eV can be assigned to Cu^{2+} ($2p_{3/2}$) and Cu^{2+} ($2p_{1/2}$)[30d] respectively. As for **3** (Figure 3), the XPS spectra exhibit two overlapped peaks at 232.1 and 235.1 eV, corresponding to Mo^{6+} ($3d_{5/2}$) and Mo^{6+} ($3d_{3/2}$), respectively; and two peaks at 855.3 and 872.4 eV can be attributed to Ni^{2+}($2p_{3/2}$) and Ni^{2+} ($2p_{1/2}$)[30e,f] respectively.These results are consistent with the structure analyses.

(30) (a) Brown, I. D.; Altermatt, D. *Acta Crystallogr., Sect. B* **1985**, *41*, 244. (b) Nefedov, V. I.; Firsov, M. N.; Shaplygin, I. S. *J. Electron Spectrosc. Relat. Phenom.* **1982**, *26*, 65. (c) Patterson, T. A.; Carver, J. C.; Leyden, D. E.; Hercules, D. M. *J. Phys. Chem.* **1976**, *80*, 1700. (d) Yu, K.; Li, Y. G.; Zhou, B. B.; Su, Z. H.; Zhao, Z. F.; Zhang, Y. N. *Eur. J. Inorg. Chem.* **2007**, 5662. (e) Yamasaki, K.; Yoshida, T. *Bull. Chem. Soc. Jpn.* **1981**, *54*, 935. (f) Beyer, L.; Kimse, R.; Stach, J.; Szargan, R.; Hoyer, E. *Z. Anorg. Allg. Chem.* **1981**, *476*, 7.

Structural Description. The experimental XRPD patterns of the bulk products of **1** and **3** are in good agreement with the simulated XRPD patterns based on the results from single-crystal X-ray diffraction, indicating the phase purity of the sample (Figure 4). The intensity difference between the experimental and simulated XRPD patterns is due to the variation in preferred orientation of the powder sample during collection of the experimental XRPD.

Structural analyses exhibit that the skeletons of **1** and **2** are made up of bi-TM-substituted sandwich-type germanomolybdate polyoxoanion $[M_2(\beta\text{-Y-GeMo}_9O_{33})_2]^{n-}$ (M = Cu^{II}, n = 12 for **1**; M = Cr^{III}, n = 10 for **2**). Different from **1** and **2**, the skeletons of **3**−**5** are composed of tetra-TM-substituted sandwich-type germanomolybdate polyoxoanion $[M_4(H_2O)_2(\alpha\text{-B-GeMo}_9O_{34})_2]^{12-}$ (M = Ni^{II} for **3**, M = Mn^{II} for **4** and M = Co^{II} for **5**). It is especially interesting that the polyoxoanions of **1** and **2** are made up of two unusual $[\beta\text{-Y-GeMo}_9O_{33}]^{8-}$ fragments whereas the polyoxoanions of **3**−**5** are built by two familiar $[\alpha\text{-B-GeMo}_9O_{34}]^{10-}$ fragments.

It is well-known that the familiar saturated α-Keggin and β-Keggin polyoxoanions can be transformed into trivacant A-type and B-type Keggin polyoxoanions through removing a corner-sharing M_3O_{13} (M = Mo^{VI}, W^{VI}) group or an edge-sharing M_3O_{13} group, respectively. In **1** and **2**, the unusual $[\beta\text{-Y-GeMo}_9O_{33}]^{8-}$ fragment

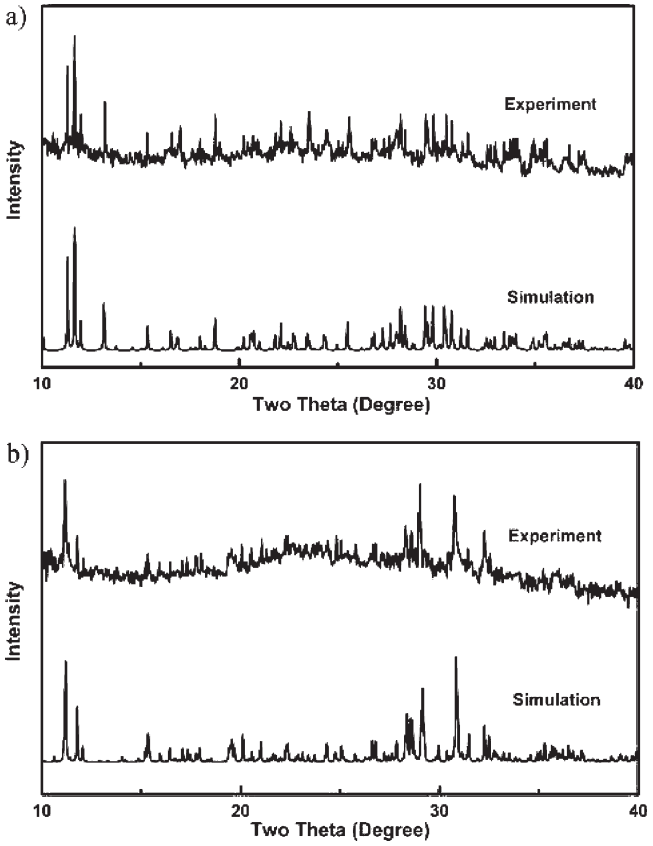

Figure 4. (a) Comparison of the simulated and experimental XRPD patterns of **1**; (b) Comparison of the simulated and experimental XRPD patterns of **3**.

Scheme 1. (a) Usual $[\beta\text{-A/B-GeMo}_9\text{O}_{33}]^{8-}$ Units and the Unusual $[\beta\text{-Y-GeMo}_9\text{O}_{33}]^{8-}$ Unit Derive from the Well-Known $[\beta\text{-GeMo}_{12}\text{O}_{40}]^{4-}$; (b) the $[\beta\text{-X-SiW}_9\text{O}_{34}]^{10-}$ Units Derive from the Well-Known $[\beta\text{-SiW}_9\text{O}_{34}]^{10-}$; (c) the Familiar $[\alpha\text{-A/B-GeMo}_9\text{O}_{34}]^{10-}$ Units Derive from the Well-Known $[\alpha\text{-GeMo}_{12}\text{O}_{40}]^{4-}$

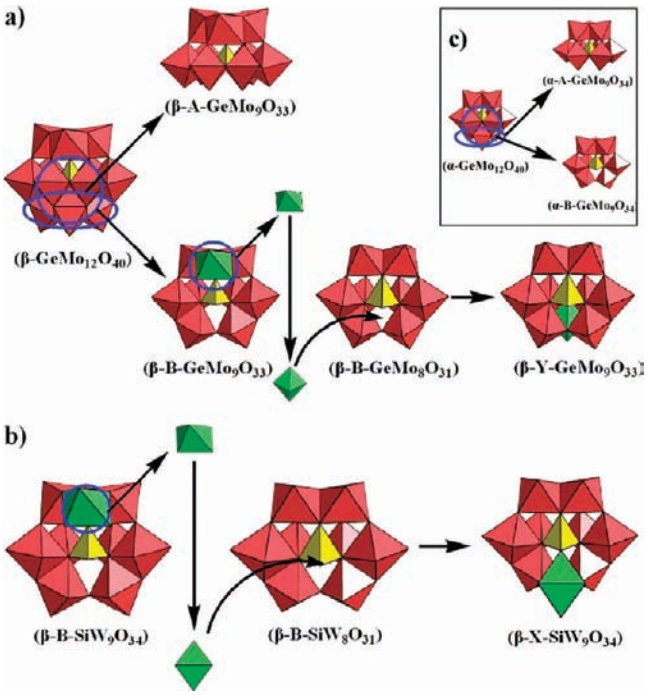

can be viewed as a derivative of the well-known $[\beta\text{-B-GeMo}_9\text{O}_{33}]^{8-}$ polyoxoanion by removing one MoO_6 octahedron on a Mo_3O_{13} group of the $[\beta\text{-B-GeMo}_9\text{O}_{33}]^{8-}$polyoxoanion to the other side of itself, and capping to a window surrounded by another two Mo_3O_{13} units (Scheme 1a).[31] This structural feature is significantly different from the β-X-type polyoxoanion $[\beta\text{-X-SiW}_9\text{O}_{34}]^{10-}$,[8d] which can be considered to be derived from the well-known $[\beta\text{-B-SiW}_9\text{O}_{34}]^{10-}$ polyoxoanion by moving one WO_6 octahedron on a W_3O_{13} group of the $[\beta\text{-B-SiW}_9\text{O}_{34}]^{10-}$ polyoxoanion to the same side itself, and capping to SiO_4 tetrahedron and two WO_6 octahedra from two W_3O_{13} groups (Scheme 1b). As is mentioned above, $[\beta\text{-Y-GeMo}_9\text{O}_{33}]^{8-}$ and $[\beta\text{-X-SiW}_9\text{O}_{34}]^{10-}$ represent two new memberships of the family of B-type trivacant Keggin anions. However, different from **1** and **2**, the familiar $[\alpha\text{-B-GeMo}_9\text{O}_{34}]^{10-}$ polyoxoanion in **3**−**5** is derived from the well-known $[\alpha\text{-GeMo}_{12}\text{O}_{40}]^{4-}$ polyoxoanion by moving an edge-sharing Mo_3O_{13} group (Scheme 1c), which is similar to the familiar α-B-$[XW_9O_{34}]^{n-}$ ($X = P^V/As^{III}/Si^{IV}/Ge^{IV}$, etc.) polyoxoanion.

Single-crystal structural analyses reveal that **1** and **2** are almost isostructural regardless of the presence of discrete countercations and **3**−**5** are completely isostructural. Therefore, only the structures of **1** and **3** are described in detail.

In **1** and **2**, the $[M_2(\beta\text{-Y-GeMo}_9\text{O}_{33})_2]^{n-}$ ($M = Cu^{II}$, $n = 12$ for **1**; $M = Cr^{III}$, $n = 10$ for **2**) polyoxoanion is composed of the association of two unusual $[\beta\text{-Y-GeMo}_9\text{O}_{33}]^{8-}$ fragments linked by two Cu^{II}/Cr^{III} ions leading to a sandwich-type structural assembly with the idealized C_{2h} point symmetry (Figure 5a). This structural feature is similar to the reported arsenomolybdate and vanadiummolybdate species (Figure 6a).[26,27] To date, the dinuclear TM substituted sandwich-type POMs are rather rare (Figure 6a, 6b).[3d,26,27] To our knowledge, **1** and **2** represent the first dinuclear TM sandwiched germanomolybdates.

The molecular structure of **1** consists of a $[Na_{12}(H_2O)_{36}]^{12+}$ cluster, a rare di-Cu^{II} substituted sandwich-type polyoxoanion $[Cu_2(\beta\text{-Y-GeMo}_9\text{O}_{33})_2]^{12-}$ and three lattice water molecules. In the polyoxoanion $[Cu_2(\beta\text{-Y-GeMo}_9\text{O}_{33})_2]^{12-}$, both Cu^{II} cations in the sandwich belt exhibit in a six-coordinate distorted octahedral geometries defined by six oxygen atoms from two $[\beta\text{-Y-GeMo}_9\text{O}_{33}]^{8-}$ fragments (Figure 5b). The corresponding Cu−O distances range from 1.935(3) to 1.983(3) Å, and the Cu1···Cu2 separation is 2.955 Å. It is notable that 12 Na^+ cations in the $[Na_{12}(H_2O)_{36}]^{12+}$ cluster are hexa-coordinate octahedra formed by 6 oxygen atoms from water molecules and polyoxoanions, which join together through face-/edge-corner-sharing to form an *S*-shaped cluster (Scheme 2a). To our knowledge, such dodecameric $[Na_{12}(H_2O)_{36}]^{12+}$ cluster is the first one observed. The most intriguing feature of **1** is that each dodecameric $[Na_{12}(H_2O)_{36}]^{12+}$ cluster (Scheme 2a) connects six $[Cu_2(\beta\text{-Y-GeMo}_9\text{O}_{33})_2]^{12-}$ polyoxoanions (Scheme 2b), meanwhile each $[Cu_2(\beta\text{-Y-GeMo}_9\text{O}_{33})_2]^{12-}$ polyoxoanion is combined with six dodecameric $[Na_{12}(H_2O)_{36}]^{12+}$ clusters. By this interconnection mode, the extended 3D framework is constructed (Scheme 2c). From the topological viewpoint,

(31) Pope, M. T. *Heteropoly and Isopoly Oxometalates*; Springer: Berlin, 1983.

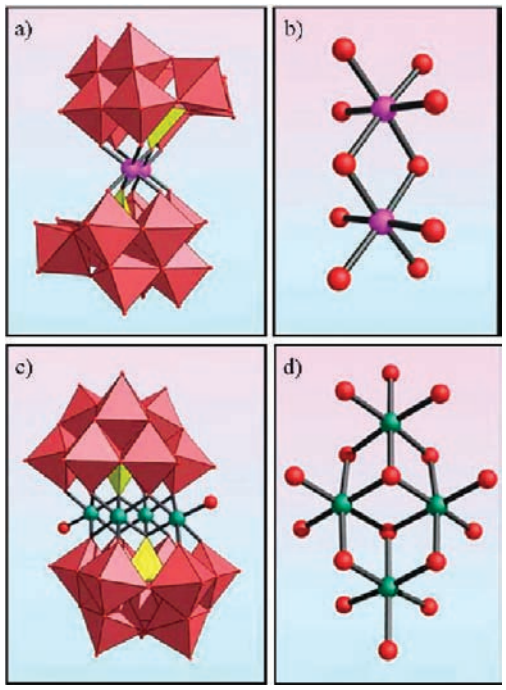

Figure 5. (a) Polyhedral and ball-and-stick illustration of $[M_2(\beta\text{-Y-GeMo}_9O_{33})_2]^{n-}$ (M = Cu^{II}, n = 12 for **1**; M = Cr^{III}, n = 10 for **2**); (b) The M_2O_{10} group sandwiched by two trivacant $[\beta\text{-Y-GeMo}_9O_{33}]^{8-}$ Keggin fragments in **1** and **2**; (c) The polyhedral and ball-and-stick illustration of $[M_4(H_2O)_2(\alpha\text{-B-GeMo}_9O_{34})_2]^{12-}$ (M = Ni^{II} for **3**, M = Mn^{II} for **4** and M = Co^{II} for **5**); (d) The rhomb-like M_4O_{16} group sandwiched by two trivacant $[\alpha\text{-B-GeMo}_9O_{34}]^{10-}$ Keggin fragments in **3**−**5**. Color codes: MoO_6, red; GeO_4, yellow; Cu/Cr, magenta; Ni/Mn/Co, green; O, red.

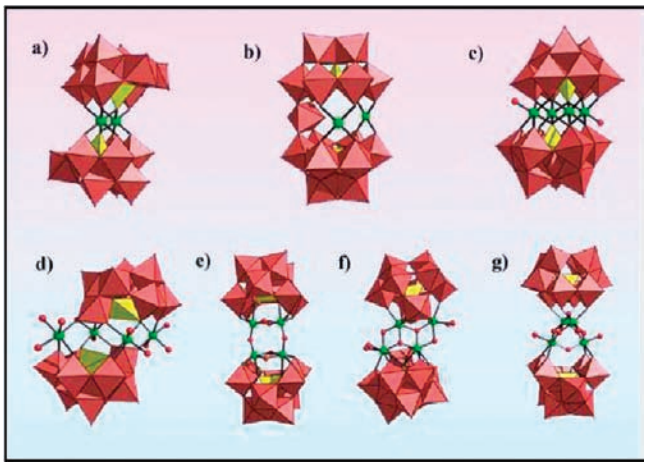

Figure 6. (a) Illustrations of some representative dinuclear (a, b) and tetranuclear (c−g) sandwich-type compounds previously reported.

when the dodecameric $[Na_{12}(H_2O)_{36}]^{12+}$ cluster and $[Cu_2(\beta\text{-Y-GeMo}_9O_{33})_2]^{12-}$ polyoxoanion are respectively viewed as a six-connected node, the extended 3D framework can be simplified to a (6, 6)-connected 3D topology (Scheme 2d). Comparing the topology of **1** with those known minerals, **1** possesses the NaCl topology. As far as we know, **1** is the first NaCl-type TM-substituted POM, although the $CdSO_4$-type and $CdSO_4$-like TM-substituted POMs have been reported by Zhao et al.[5d,5e] **2** displays a similar polyoxoanion structure to **1**; however, the apparent difference is that the adjacent bi-Cr^{III}-substituted sandwich-type $[Cr_2(\beta\text{-Y-GeMo}_9O_{33})_2]^{10-}$

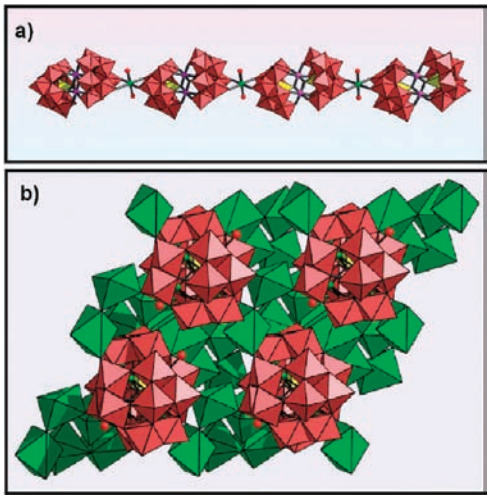

Figure 7. (a) 1D chain in the crystallographic bc plane of **2**; (b) the 3D structures of **3**−**5** along ab plane. Color codes: MoO_6, red; GeO_4, yellow; NaO_6, light green. Cr, magenta; Na, light green; O, red.

polyoxoanions connect each other via $[Na(H_2O)_2]^+$ bridges constructing an 1D chain along the *a* axis (Figure 7a).

The polyoxoanion $[Ni_4(H_2O)_2(\alpha\text{-B-GeMo}_9O_{34})_2]^{12-}$ of **3** is constructed from two unprecedented $[\alpha\text{-B-GeMo}_9O_{34}]^{10-}$ fragments linked by a rhomb-like Ni_4O_{16} group leading to a sandwich-type structure with C_{2h} point symmetry (Figure 5c). As is shown in Figure 5d, the rhomb-like $\{Ni_4O_{16}\}$ group contains four edge-sharing Ni^{II} octahedra. The four Ni^{2+} ions are all octahedrally coordinate. Two of them are situated in two internal positions and coordinated by two $[\alpha\text{-B-GeMo}_9O_{34}]^{10-}$ fragments; the remaining two Ni^{2+} ions are in two external positions and bonded by terminal water ligands and two $[\alpha\text{-B-GeMo}_9O_{34}]^{10-}$ fragments. The relevant Ni−O distances vary from 2.011(3) to 2.093(3) Å, and the independent Ni···Ni separations are 3.095 Å, 3.097 Å, 3.098 Å, 5.362 Å, respectively. The results show that significant potential magnetic interactions between the Ni^{2+} ions in the $\{Ni_4O_{16}\}$ group maybe exist. In **3**, a notable feature is that polyoxoanions $[Ni_4(H_2O)_2(\alpha\text{-B-GeMo}_9O_{34})_2]^{12-}$ are connected by discrete Na^+ cations yielding a 3D structure (Figure 7b).

To the best of our knowledge, the reported tetranuclear-substituted sandwich-type HPTs mainly contain five structural types. The most familiar rhomb-like tetra-TM substituted sandwich type (Figure 6c) was first found by Weakley et al.[3g] In 1998, Krebs reported a rare tetra-Mn^{II}-substituted sandwich-type telluriumtungstate (Figure 6d).[6a] In 2006, Mizuno synthesized a novel cyclic tetra-Ti^{IV} substituted silicotungstate $[\{\gamma\text{-SiTi}_2W_{10}O_{36}(OH)_2\}_2(\mu\text{-O})_2]^{8-}$[32a] (Figure 6e). In the same year, Kortz addressed another rhomb-like tetra-TM substituted sandwich type $[Zr_4O_2(OH)_2(H_2O)_4(\beta\text{-SiW}_{10}O_{37})_2]^{10-}$[8b] (Figure 6f). Recently, Sartorel's group prepared a tetrahedral tetra-Ru^{IV} substituted sandwich-type silicotungstate $[Ru_4(\mu\text{-O})_4(\mu\text{-OH})_2(H_2O)_4(\gamma\text{-SiW}_{10}O_{36})_2]^{10-}$ (Figure 6g).[32b] However, it should be mentioned that no tetra-TM substituted sandwich-type HPM analogue has been reported to date; thus, **3**−**5** exhibit the first reported HPMs with tetra-TM substituted sandwich-type structures.

Thermal Properties. The thermal properties of **1**−**3** (Supporting Information, Figure S8) have been measured

Scheme 2. (a) Distribution of the *S*-Shaped $[Na_{12}(H_2O)_{36}]^{12+}$ Clusters in the *ab* Plane; (b) the Distribution of the $[Cu_2(\beta\text{-Y-GeMo}_9O_{33})_2]^{12-}$ Polyoxoanions in the *ab* Plane; (c) the Polyhedral Illustration of the 3D Framework Structure of **1** Viewed down the *c*-Axis; (d) the 3D NaCl-Type Topological Framework of **1**[a]

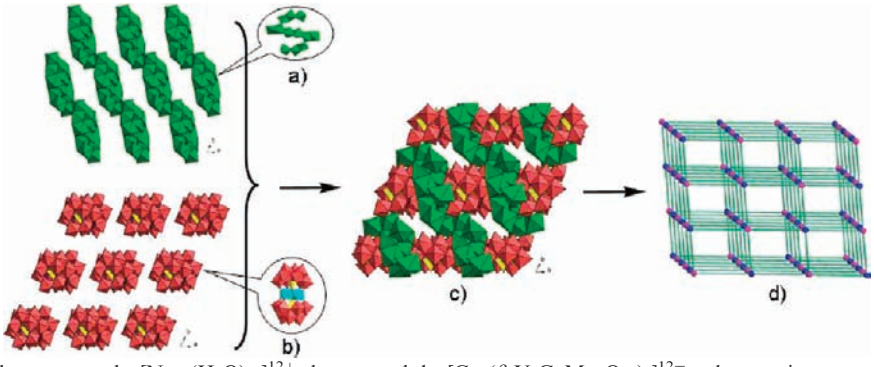

[a] Blue and magenta balls represent the $[Na_{12}(H_2O)_{36}]^{12+}$ clusters and the $[Cu_2(\beta\text{-Y-GeMo}_9O_{33})_2]^{12-}$ polyoxoanions, respectively.

in N_2 flow with a heating rate of 10 °C min^{-1} from 25 to 800 °C. The thermogravimetry (TG) curves of **1** and **3** indicate one slow step of weight loss while the weight loss of **2** can be divided into two steps. In case of **1**, the total weight loss 18.64% can be assigned to the removal of 3 lattice water molecules and 36 coordinate water molecules (calcd. 17.42%). For **2**, the weight loss of 13.19% during the first step from 25 to 466 °C involves the loss of 7 lattice water molecules and 24 coordinate water molecules (calcd. 13.87%). On further heating, the materials lose weight continuously during the second step with the weight loss of 7.14% from 466 to 800 °C, corresponding to the removal of 4 $[N(CH_3)_4]^+$ (calcd. 7.37%). As for **3**, the TG curve giving a total loss of 15.17% in the range of 25−800 °C corresponds to the release of 6 lattice water molecules, 27 coordinate water molecules, and the dehydration of 1 proton (calcd. 14.93%). The above-mentioned analyses reveal that the experimental values are approximately consistent with the theoretical values.

Surface Photovoltage Spectroscopy. The surface photovoltage (SPV) method, with a very high sensitivity, is a well-established contactless and nondestructive technique for semiconductor characterization that relies on analyzing illumination-induced changes in the surface voltage.[33a−e] The photovoltage generation mainly arises from the creation of electron−hole pairs, followed by the separation under a built-in electric field (also called space-charge layer).[33f] The SPS is an effective tool to investigate the photophysics of excited states generated by absorption in the aggregate state;[33g] it can reflect photogenerated charge separation and transfer behavior as well as optical absorption characteristics of semiconductor samples, especially for the EFISPS method, in which the SPS is combined with the electric-field-modified technique.[33h]

A signal detected by SPS is equivalent to the change in the surface potential barrier on illumination (δV_s), which is given by the equation $\delta V_s = V_s' - V_s^0$, where V_s^0 and V_s' are respectively the surface potential barriers before and after illumination.[34a] In the present paper, the SPS and EFISPS of **1** and **3** are measured to investigate the behavior of photogenerated electrons and the photoelectric property under the effect of the external electric fields. Figure 8 shows the EFISPS of **1** and **3** in the range of 300−600 nm when the external electric fields are −2, −1, 0, +1, and +2 V, respectively. In Figure 8, there are three interesting points worthy of discussion. First, the SPV values of **1** and **3** are very weak in the absence of an external electric field. Second, when a positive electric field is employed, the SPS response intensity markedly rises with increasing field strength, which is attributed to the same direction of added-outer as built-in field.[37b] In addition, with a positive electric field, the built-in field is enhanced, which leads to the increase of the diffusion length among electrons in the conduction band; thus, more electrons reach the surface, which results in the strengthening of the response of photovoltage.[34c] Third, when a negative electric field is applied, the SPS response intensity decreases and is much lower than that without electric field. This is because electrons in the conduction band move toward the bulk as a negative electric field is used; therefore, the SPV response intensity decreases.[34c] From Figure 8, it is obvious that each sample displays a pronounced SPV response band in the range of 300−450 nm, which is assigned to the exciton transition.[33a,34d] Furthermore, it is found that the bands gradually red shift with increasing strength of the positive electric fields. The explanation for the phenomenon based on the Stark effect model is followed:[34e] the electrons in bulk on the irradiated side of the electrode move to the surface on the same side of the sample under the inducement of the

(32) (a) Goto, Y.; Kamata, K.; Yamaguchi, K.; Uehara, K.; Hikichi, S.; Mizuno, N. *Inorg. Chem.* **2006**, *45*, 2347. (b) Sartorel, A.; Carraro, M.; Scorrano, G.; Zorzi, R. D.; Geremia, S.; McDaniel, N. D.; Bernhard, S.; Bonchio, M. *J. Am. Chem. Soc.* **2008**, 5006.

(33) (a) Lin, Y. H.; Wang, D. J.; Zhao, Q. D.; Yang, M.; Zhang, Q. L. *J. Phys. Chem. B* **2004**, *108*, 3202. (b) Kronik, L.; Shapira, Y. *Surf. Sci. Rep.* **1999**, *37*, 1. (c) Jing, L. Q.; Fu, H. G.; Wang, B. Q.; Wang, D. J.; Xin, B. F.; Li, S. D.; Sun, J. Z. *Appl. Catal., B* **2006**, *62*, 282. (d) Lenzmann, F.; Krueger, J.; Burnside, S.; Brooks, K.; Gratzel, M.; Gal, D.; Ruhle, S.; Cahen, D. *J. Phys. Chem. B* **2001**, *105*, 6347. (e) Xin, B. F.; Jing, L. Q.; Ren, Z. Y.; Wang, B. Q.; Fu, H. G. *J. Phys. Chem. B* **2005**, *109*, 2805. (f) Jing, L. Q.; Xin, B. F.; Yuan, F. L.; Xue, L. P.; Wang, B. Q.; Fu, H. G. *J. Phys. Chem. B* **2006**, *110*, 17860. (g) Kohler, A.; Gruner, J.; Friend, R. H.; Mullen, K.; Scherf, U. *Chem. Phys. Lett.* **1995**, *243*, 456. (h) Wang, D. J.; Zhang, J.; Shi, T. S.; Wang, B. H.; Cao, X. Z.; Li, T. J. *J. Photochem. Photobiol. A* **1996**, *93*, 21.

(34) (a) Donchev, V.; Kirilov, K.; Ivanov, T.; Germanova, K. *Mater. Sci. Eng. B.* **2006**, *129*, 186. (b) Jing, L. Q.; Sun, X. J.; Shang, J.; Cai, W. M.; Xu, Z. L.; Du, Y. G.; Fu, H. G. *Sol. Energy Mater. Sol. Cells* **2003**, *79*, 133. (c) Qi, M. H.; Liu, G. F. *J. Phys. Chem. B* **2003**, *107*, 7640. (d) Lin, Y. H.; Wang, D. J.; Zhao, Q. D.; Li, Z. H.; Ma, Y. D.; Yang, M. *Nanotech.* **2006**, *17*, 2110. (e) Dijken, A. V.; Meulenkamp, E. A.; Vanmaekelbergh, D.; Meijerink, A. *J. Phys. Chem. B* **2000**, *104*, 4355. (f) He, T.; Yao, J. N. *J. Mater. Chem.* **2007**, *17*, 4547. (g) Li, B.; Yan, Y.; Li, F. Y.; Xu, L.; Bi, L. H.; Wu, L. X. *Inorg. Chim. Acta* **2009**, *362*, 2796.

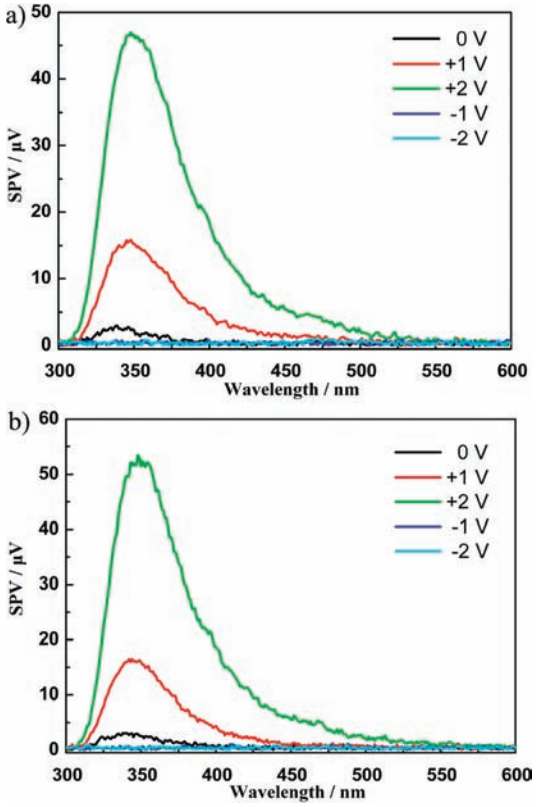

Figure 8. (a) SPS of **1** under zero and different positive and negative electric fields; (b) SPS of **3** under zero and different positive and negative electric fields.

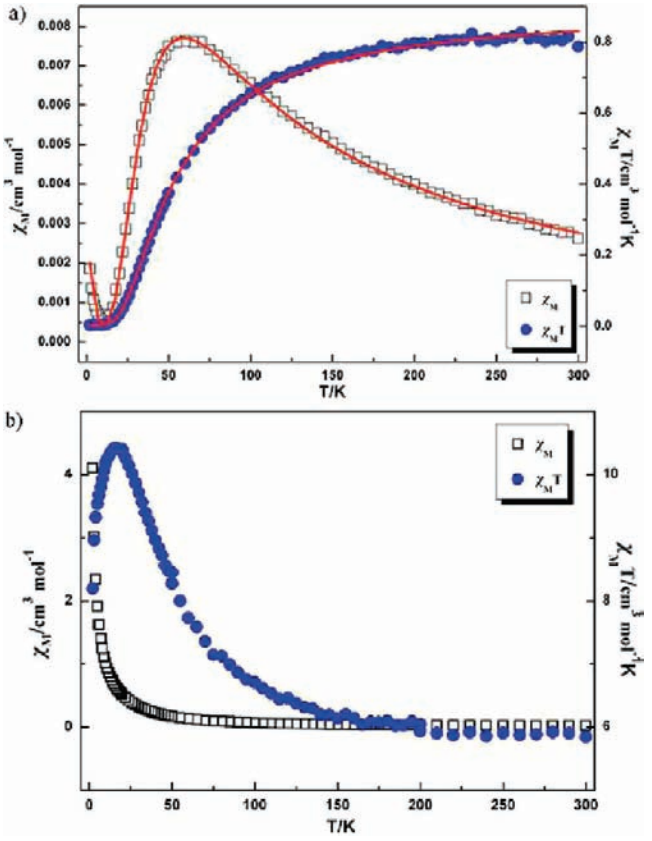

Figure 9. (a) Temperature dependence of the χ_M and $\chi_M T$ for polycrystalline samples of **1** at a 1 kOe applied field; (b) Temperature dependence of the χ_M and $\chi_M T$ for polycrystalline samples of **3** at a 2 kOe applied field.

positive electric field. With increasing electric field strength, the electron density at the top of the valence band is enhanced. The addition of state density will increase the probability of excited transitions, leading to the red shift phenomenon.[33a] In general, the behavior is that increased positive electric field results in increase in the SPV response intensity; meanwhile a decrease in the negative electric fields leads to a decrease in the SPV response intensity, indicating that **1** and **3** are the *n*-type conduction characteristic.[33a,34f] A similar phenomenon is also observed in the POM system.[34g]

Magnetic Properties. The magnetic susceptibilities of **1** and **3** were obtained on polycrystalline samples in the temperature range 2−300 K. The temperature dependence of χ_M and $\chi_M T$ product of **1** is shown in Figure 9a. Upon cooling, the χ_M value gradually increases to a maximum of 7.71×10^{-3} cm^3 mol^{-1} at 59 K, and then rapidly decreases to a minimum of 4.77×10^{-4} cm^3 mol^{-1} at 10 K, when the temperature is further lowered, a sudden increase of the χ_M value occurs which can be ascribed to some paramagnetic impurities.[35] The $\chi_M T$ product at room temperature is 0.79 cm^3 mol^{-1} K, in good agreement with the expected spin-only value of 0.75 cm^3 mol^{-1} K for two isolated Cu^{II} ions ($S = {}^1/_2$) assuming $g = 2.00$. With decreasing temperature, the $\chi_M T$ value decreases slowly up to 105 K then sharply to 0.01 cm^3 mol^{-1} K at 10 K, indicating a characteristic antiferromagnetic coupling magnetic behavior.

To evaluate the magnetic exchange interaction between Cu^{II} ions, the magnetic susceptibility data (2−300 K) were fitted by the modified Bleaney−Bowers equation for two coupled Cu^{II} ions ($S = {}^1/_2$) with the Hamiltonian in the form $H = -J\tilde{S}_1\tilde{S}_2$.[36] The susceptibility equation for such a sandwich-type system can be written as follows:[37]

$$\chi = \frac{2Ng^2\beta^2}{kT}[3+\exp(-J/kT)]^{-1}(1-\rho)+\frac{Ng^2\beta^2}{2kT}\rho \quad (1)$$

where J is an exchange constant between Cu^{II} ions, and N, g, β, and ρ parameters have their usual meaning. The best-fitting parameters obtained were $J = -66.04$ cm^{-1}, $g = 2.20$, and $\rho = 4.40 \times 10^{-3}$. At high temperature ($T >$ 104 K), the magnetic susceptibility data can be simulated by the Curie−Weiss expression with $C = 0.94$ cm^3 mol^{-1} K and $\theta = -41.97$ K (Figure 10a). The negative J and θ values further consolidate the presence of the antiferromagnetic coupling between Cu^{II} ions bridged by two μ-oxo donors in **1**.

Extensive experimental and theoretical studies performed on the spin exchanges within $[Cu_2O_2]$ units constituted by

(35) (a) Bencini, A.; Dei, A.; Sangregorio, C.; Totti, F.; Vaz, M. G. F. *Inorg. Chem.* **2003**, *42*, 8065. (b) Mikuriya, M.; Minowa, K.; Nukada, R. *Bull. Chem. Soc. Jpn.* **2002**, *75*, 2595. (c) Thompson, L. K.; Mandal, S. K.; Tandon, S. S.; Bridson, J. N.; Park, M. K. *Inorg. Chem.* **1996**, *35*, 3117.

(36) Koner, S.; Saha, S.; Mallah, T.; Okamoto, K. I. *Inorg. Chem.* **2004**, *43*, 840.

(37) Kahn, O. *Molecular Magnetism*; VCH Publishers: New York, 1993; p 132.

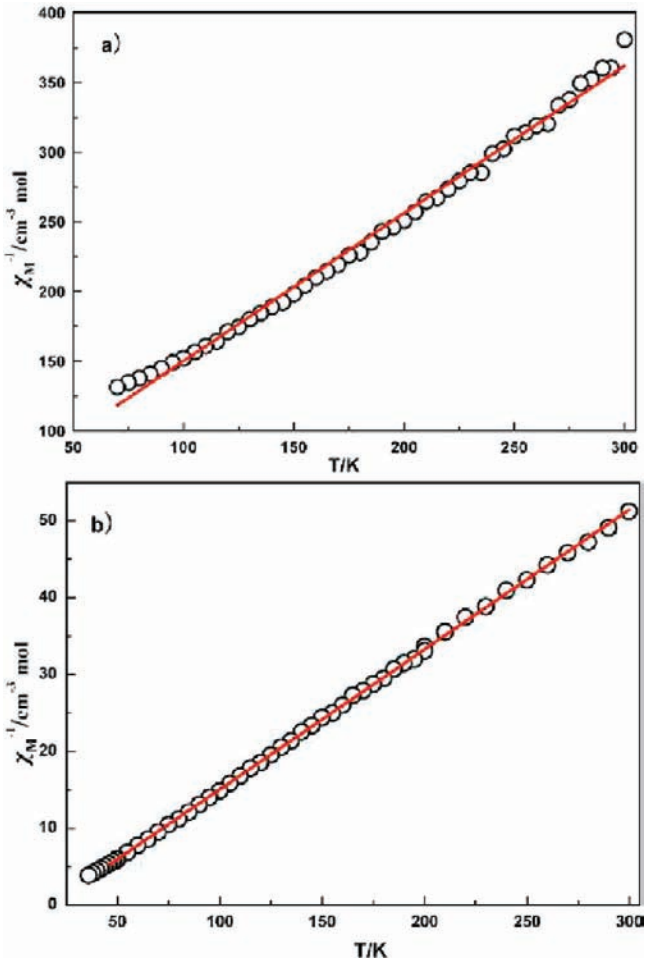

Figure 10. (a) Temperature evolution of the inverse magnetic susceptibility χ_M^{-1} for **1** (a) between 50 and 300 K, and **3** (b) between 25 and 300 K. The red solid lines are generated from the best fit by the Curie−Weiss expression with the Curie constant $C = 0.94$ cm^3 mol^{-1} K and the Weiss constant $\theta = -41.97$ K for **1** and the Curie constant $C = 5.49$ cm^3 mol^{-1} K and the Weiss constant $\theta = 17.16$ K for **3**.

hydroxide[38] and alkoxide[39] bridges show that the magnetic interactions are highly sensitive to the values of the Cu−O−Cu bridging angles (α) and conclude a correlation between the experimental exchange constants and the Cu−O−Cu bond angles: the compounds are generally antiferromagnetic for $\alpha > 98°$, whereas ferromagnetic for $\alpha < 98°$.[3f,40] The fact that the Cu−O−Cu angle of 98.8(1)° in **1** is slightly larger than 98° indicates that the weak antiferromagnetic interactions are expected in accordance with the simulated results.

Figure 9b shows the magnetic behavior of **3** in the plots of the χ_M and $\chi_M T$ product versus T. The χ_M shows a constant of 0.028 cm^3 mol^{-1} with a slight increase between 300 and 50 K, and then exponentially reaches the maximum of 4.11 cm^3 mol^{-1} at 2 K. The $\chi_M T$ product continuously increases with decreasing temperature from 5.85 cm^3 mol^{-1} K at 300 K to a maximum of 10.42 cm^3 mol^{-1} K at 16 K. This behavior demonstrates dominant ferromagnetic interactions among magnetic centers. The sharp drop in the $\chi_M T$ value below the apex temperature suggests the presence of significant zero-field splitting (ZFS) effects in the ground state or molecular interactions.[41] It is worth noting that in previous work, investigators showed that the behavior of $\chi_M T$ at very low temperatures may be related to an anisotropic coupling of the Ni^{II} ions inside the cluster rather than to a mean-field correction.[42] The temperature dependence of the inverse susceptibilities ($1/\chi_M$) obeys the Curie−Weiss law above 45 K affording $C = 5.49$ cm^3 mol^{-1} K and $\theta = 17.16$ K (Figure 10b). The positive Weiss constant also supports the presence of the ferromagnetic exchange interactions between adjacent Ni^{II} centers mediated by the oxygen bridges. Such ferromagnetic coupling in the rhombic Ni_4O_{16} cluster unit has been observed in $\{[Ni(dap)(H_2O)]_2[Ni(dap)_2]_2[Ni_4(Hdap)_2(B\text{-}\alpha\text{-}HSiW_9O_{34})_2]\}\cdot 7H_2O$,[3e] $\{[Ni(dap)_2(H_2O)]_2[Ni(dap)_2]_2[Ni_4(Hdap)_2(B\text{-}\alpha\text{-}HGeW_9O_{34})_2]\}\cdot 6H_2O$,[3e] $K_6Na_4[Ni_4(H_2O)_2(B\text{-}\alpha\text{-}PW_9O_{34})_2]\cdot 24H_2O$,[7e] and $[Ni_4(\mu_3\text{-}OH)_2(H_2O)_6(ntp)_2]\cdot 2H_2O$ ($H_3ntp = N(CH_2CH_2COOH)_3$).[41a] According to the previous study, the magnetic interactions are highly sensitive to the values of the Ni−O−Ni bridging angles: the interactions are ferromagnetic for angles in the range of 90 ± 14°, whereas they are antiferromagnetic for larger angles.[7e,42,43] In fact, all the Ni−O−Ni bond angles are between 95.8° and 98.1° in **3**, therefore, dominant ferromagnetic exchange interactions are not unexpected. Besides ferromagnetic couplings in tetra-Ni^{II} sandwiched POMs, ferromagnetic exchange interactions in the cubane Ni_4O_4 cluster unit in $Cs_2[H_2PW_9Ni_4O_{34}(OH)_3(H_2O)_6]\cdot 5H_2O$ have been reported by Kortz et al.[44] Moreover, the ferromagnetic coupling interactions in the coplanar hexa-Ni^{II} cluster substituted polyoxotungstates were investigated by Yang et al.[3f,5c]

Conclusions

In this paper, two types of rare sandwich-type germanomolybdates have been synthesized using a rational one-pot synthetic strategy. **1** and **2** display the rare dinuclear TM substituted sandwich-type with unusual trivacant {β-Y-$GeMo_9O_{33}$} germanomolybdate units whereas **3**−**5** exhibit the first tetranuclear TM substituted sandwich-type with familiar trivacant {α-B-$GeMo_9O_{34}$} germanomolybdate units. SPS and EFISPS measurements reveal that **1** and **3** have the behavior of an *n*-type semiconductor. Magnetic properties show that **1** and **3** demonstrate the antiferromagnetic coupling and ferromagnetic exchange interactions, respectively. Further work in this area will be focus on making other novel high-nuclear

(38) Crawford, V. H.; Richardson, H. V.; Wason, J. R.; Hodgson, D. J.; Hatfield, W. E. *Inorg. Chem.* **1976**, *15*, 2107.
(39) (a) Merz, L.; Haase, W. *J. Chem. Soc., Dalton Trans.* **1980**, 875. (b) Handa, M.; Koga, N.; Kida, S. *Bull. Chem. Soc. Jpn.* **1988**, *61*, 3853.
(40) (a) Ruiz, E.; Alemany, P.; Alvarez, S.; Cano, J. *J. Am. Chem. Soc.* **1997**, *119*, 1297. (b) Aroméí, G.; Ribas, J.; Gamez, P.; Roubeau, O.; Kooijman, H.; Spek, A. L.; Teat, S.; MacLean, E.; Stoeckli-Evans, H.; Reedijk, J. *Chem.—Eur. J.* **2004**, *10*, 6476. (c) Shores, M. P.; Bartlett, B. M.; Nocera, D. G. *J. Am. Chem. Soc.* **2005**, *127*, 17986.
(41) (a) King, P.; Clérac, R.; Wernsdorfer, W.; Anson, C. E.; Powell, A. K. *Dalton Trans.* **2004**, 2670. (b) Fondo, M.; Ocampo, N.; García-Deibe, A. M.; Vicente, R.; Corbella, M.; Bermejo, M. R.; Sanmartín, J. *Inorg. Chem.* **2006**, *45*, 255. (c) Serna, Z. E.; Lezama, L.; Urtiaga, M. K.; Arriortua, M. I.; Barandika, M. G.; Cortés, R.; Rojo, T. *Angew. Chem., Int. Ed.* **2000**, *39*, 344.
(42) Mbomekalle, I. M.; Keita, B.; Nierlich, M.; Kortz, U.; Berthet, P.; Nadjo, L. *Inorg. Chem.* **2003**, *42*, 5143.
(43) Bertrand, J. A.; Ginsberg, A. P.; Kaplan, R. I.; Eirkwood, K. C.; Martin, R. L.; Sherwood, R. C. *Inorg. Chem.* **1971**, *10*, 240.
(44) Kortz, U.; Tézé, A.; Hervé, G. *Inorg. Chem.* **1999**, *38*, 2038.

metal cluster aggregations by adopting appropriate reaction conditions.

Acknowledgment. We thank the National Natural Science Foundation of China, Program for New Century Excellent Talents in University of Henan Province, the Foundation of Education Department of Henan Province and Natural Science Foundation of Henan Province for financial support.

Supporting Information Available: The comparison of IR data between crystal phase and powder phase of **2**; IR spectra of **1**−**5**; IR spectrum of the powder of **2**; UV spectra of **1**−**5**; the solid state UV spectra of **1** and **3**; comparison between the UV spectra of **1** and the UV spectrum of $Na_2MoO_4 \cdot 2H_2O$; the influence of the pH values on the stability of **3** in aqueous solution; TG curves of **1**−**3**; crystal data in CIF format. This material is available free of charge via the Internet at http://pubs.acs.org.